Valence-band satellite in ferromagnetic nickel: LDA + DMFT study with exact diagonalization

Jindřich Kolorenč,[1,2,*] Alexander I. Poteryaev,[3,4] and Alexander I. Lichtenstein[1]

[1]*Institut für Theoretische Physik, Universität Hamburg, Jungiusstraße 9, D-20355 Hamburg, Germany*

[2]*Institute of Physics, Academy of Sciences of the Czech Republic, Na Slovance 2, CZ-182 21 Praha 8, Czech Republic*

[3]*Institute of Metal Physics, Russian Academy of Sciences, 620990 Ekaterinburg, Russia*

[4]*Institute of Quantum Materials Science, 620107 Ekaterinburg, Russia*

(Received 1 March 2012; published 20 June 2012)

The valence-band spectrum of the ferromagnetic nickel is calculated using the LDA + DMFT method. The auxiliary impurity model emerging in the course of the calculations is discretized and solved with the exact diagonalization, or, more precisely, with the Lanczos method. Particular emphasis is given to spin dependence of the valence-band satellite that is observed around 6 eV below the Fermi level. The calculated satellite is strongly spin polarized in agreement with experimental findings.

DOI: 10.1103/PhysRevB.85.235136 PACS number(s): 71.20.Be, 71.15.−m, 75.30.−m

I. INTRODUCTION

The electronic structure of transition metals has been intensively studied for a number of decades. Notwithstanding, certain aspects of the electron behavior in these materials are still not completely understood. Comparison of experimental findings with one-electron band theories have indicated that a more thorough treatment of quantum many-body effects is necessary to accurately describe the physical reality.

A prototypical metal displaying pronounced electron correlations is the ferromagnetic nickel: its one-particle spectrum obtained using the local-density approximation (LDA) to the density-functional theory (DFT) noticeably departs from the spectra measured in photoemission experiments. The calculated $3d$ bandwidth as well as the exchange splitting are too large.[1,2] Moreover, the LDA completely misses the satellite feature located at approximately 6 eV below the Fermi level.[3–5] This satellite was originally attributed to plasmon excitations,[4] but an alternative view was soon proposed,[6,7] according to which the satellite is a result of a correlated state of two $3d$ holes localized in a single atom. The latter picture is supported by a resonant enhancement of the satellite that is observed when a second scattering channel involving $3p$ electrons and ending in the same two-hole final state becomes active.[8–10] The link between the satellite and the localized two-hole states can be explicitly visualized in simplified finite-sized models that allow for an exact many-body solution.[11,12]

A quantitative description of the electron correlations in nickel can be achieved by incorporating a dynamical self-energy into the LDA or Hartree-Fock band structure.[13–15] Usually, the self-energy is assumed local, that is, wave-vector independent. The most sophisticated local self-energy is provided by the dynamical-mean-field theory (DMFT)[16] that maps the problem of interacting lattice electrons onto an impurity model where the interactions are retained only at a single lattice site. The combination of LDA and DMFT (the so-called LDA + DMFT method) was applied to the electronic structure of nickel several times in the past, using different methods to solve the auxiliary impurity model.[17–21] A reasonable description was achieved employing the Hirsch-Fye quantum Monte Carlo (QMC) method as the impurity solver.[17] The QMC methods have many merits. In particular, they are consistently accurate regardless of the strength of correlations in the system. But they have weaknesses too. The QMC calculations of the one-particle spectral functions involve a numerical continuation from the imaginary time to the real frequencies, a procedure with a limited resolution especially at higher binding energies. Additionally, the QMC algorithm used in Ref. 17 is limited to a diagonal-only Coulomb interaction. This truncated interaction breaks a subset of symmetries characteristic for the full Coulomb operator, which can lead to undesirable side effects.

In this paper we solve the auxiliary impurity model of the LDA + DMFT by means of the Lanczos method. This strategy involves a discretization of the impurity model, which represents an obvious limitation on the achievable accuracy. The sources of errors in this approach are, however, very different from those in the QMC method and the two impurity solvers can thus offer complementary information. Using the Lanczos method, the one-particle Green's function can be evaluated directly anywhere in the complex plane without resorting to any extrapolation.

II. METHOD

We start from the bare electronic structure of Ni expressed in terms of a tight-binding LMTO model[22] containing $4s$, $3d$, and $4p$ electronic states. The one-electron Hamiltonian $\hat{H}(\mathbf{k})$ is obtained as a solution of the local-density approximation and the correlations beyond this approximation are accounted for by a local self-energy $\hat{\Sigma}$ acting in the subspace of the d orbitals. The self-energy is spin polarized, whereas the Hamiltonian $\hat{H}(\mathbf{k})$ is spin independent.

The self-energy $\hat{\Sigma}$ is constructed with the aid of an impurity model defined by a Hamiltonian $\hat{H}_{\mathrm{imp}} = \hat{H}^{(0)}_{\mathrm{imp}} + \hat{U}$ that describes a single d shell hybridized with a sea of auxiliary conduction electrons. These auxiliary electrons, often referred to as the bath, model the environment around the d shell in the actual nickel lattice. The Coulomb interaction $\hat{U}$ acts only among the d orbitals and the one-particle part $\hat{H}^{(0)}_{\mathrm{imp}}$ has the form

$$\hat{H}^{(0)}_{\mathrm{imp}} = \sum_{m\sigma} \epsilon_{m\sigma} \hat{d}^{\dagger}_{m\sigma} \hat{d}_{m\sigma} + \sum_{km\sigma} \epsilon_{km\sigma} \hat{c}^{\dagger}_{km\sigma} \hat{c}_{km\sigma} + \sum_{km\sigma} V_{km\sigma} (\hat{d}^{\dagger}_{m\sigma} \hat{c}_{km\sigma} + \hat{c}^{\dagger}_{km\sigma} \hat{d}_{m\sigma}), \quad (1)$$

where $\hat{d}^\dagger_{m\sigma}$ creates an electron in the d shell and $\hat{c}^\dagger_{km\sigma}$ creates a conduction electron in the bath. The index m runs over $e_g = \{x^2-y^2, z^2\}$ and $t_{2g} = \{xy, xz, yz\}$ states, and $\sigma \in \{\uparrow, \downarrow\}$ labels spin projections. The hybridization parameters $V_{km\sigma}$ couple only those impurity and bath levels that carry the same indices m and σ, and hence the cubic symmetry and the electron spins are preserved.

Provided we can solve the interacting impurity model, the self-energy $\hat{\Sigma}$ is obtained as

$$\hat{\Sigma} = \hat{G}^{-1}_{\rm imp}\big[\hat{H}^{(0)}_{\rm imp}\big] - \hat{G}^{-1}_{\rm imp}[\hat{H}_{\rm imp}], \tag{2a}$$

where $\hat{G}_{\rm imp}[\hat{H}]$ represents the Green's function matrix in the d-orbital subspace evaluated for a general impurity Hamiltonian $\hat{H}$. The matrix $\hat{G}_{\rm imp}[\hat{H}^{(0)}_{\rm imp}]$, which we will denote as $\hat{\mathcal{G}}$ for short, is usually referred to as the bath Green's function. The link between the original lattice electrons and the parameters entering the Hamiltonian $\hat{H}^{(0)}_{\rm imp}$ is provided by the condition

$$\hat{G}_{\rm imp}[\hat{H}_{\rm imp}] = \hat{G}[\hat{H}(\mathbf{k}), \hat{\Sigma}] \tag{2b}$$

that equates $\hat{G}_{\rm imp}$ to the local d-orbital Green's function $\hat{G}$ evaluated in the lattice. The right-hand side of Eq. (2b) can be expressed as a momentum sum over the first Brillouin zone

$$\hat{G}(z) = \frac{1}{N}\sum_k [(z+\mu)\hat{I} - \hat{H}(\mathbf{k}) - \hat{\Sigma}(z)]^{-1}, \tag{3}$$

where $\hat{I}$ stands for the identity operator and the chemical potential μ is chosen such that the $4s$-$3d$-$4p$ space holds ten electrons per Ni atom.

Equations (2) define the dynamical-mean-field approximation. They are iteratively solved for $\hat{\Sigma}$ and $\hat{H}^{(0)}_{\rm imp}$ while $\hat{H}(\mathbf{k})$ and $\hat{U}$ act as inputs. The most involved part of these iterations is the solution of the multi-orbital impurity model, for which we employ the following approximation: we discretize the impurity Hamiltonian $\hat{H}_{\rm imp}$ and then solve the resulting finite-sized cluster $\hat{H}_{\rm c}$ essentially exactly by means of the Lanczos method. This strategy was successfully applied to the DMFT equations for the repulsive[16,23] and attractive[24] single-band Hubbard models as well as for realistic multiband problems.[25] The discretization $\hat{H}_{\rm imp} \to \hat{H}_{\rm c}$ amounts to a replacement of the infinite sums (integrals) over k in Eq. (1) with short finite sums $\sum_{k=1}^{N_k}$. If not explicitly stated otherwise, we use $N_k = 2$, in other words, each impurity orbital is coupled to two bath orbitals.

The parameters of the discretized Hamiltonian ($\epsilon_{m\sigma}$, $\epsilon_{km\sigma}$, and $V_{km\sigma}$) are expressed as functions of $\hat{H}(\mathbf{k})$ and $\hat{\Sigma}$ with the aid of the relation

$$\hat{\mathcal{G}}^{-1}_{\rm c} \equiv \hat{G}^{-1}_{\rm imp}\big[\hat{H}^{(0)}_{\rm c}\big] \approx \hat{G}^{-1}[\hat{H}(\mathbf{k}), \hat{\Sigma}] + \hat{\Sigma} = \hat{\mathcal{G}}^{-1}, \tag{4}$$

which is just a rearranged form of Eqs. (2). It is, of course, necessary to specify in what sense the discrete bath Green's function $\hat{\mathcal{G}}_{\rm c}$ approximates the continuous function $\hat{\mathcal{G}}$, that is, to define the precise meaning of the symbol $\approx$ in Eq. (4).

It has become customary to minimize some distance between $\hat{\mathcal{G}}_{\rm c}(z)$ and $\hat{\mathcal{G}}(z)$ defined on the Matsubara frequencies $z = i\omega_n$. A particularly convenient choice is the least-squares fit[16,23–25]

$$\min_{\substack{\epsilon_{m\sigma},\epsilon_{km\sigma},\\ V_{km\sigma}}} \sum_n \left| \frac{1}{\mathcal{G}^{\rm c}_{m\sigma}(i\omega_n)} - \frac{1}{\mathcal{G}_{m\sigma}(i\omega_n)} \right|^2 \tag{5}$$

for each m and σ. Initially we used this method of bath discretization, but we ran into unexpected difficulties. We have observed that Eq. (5) often places some of the bath energies $\epsilon_{km\sigma}$ quite far from the Fermi level due to a large high-frequency tail of the function to be fitted. That by itself would not be an issue if it did not lead to an unphysical stabilization of a nonmagnetic solution for $N_k = 2$; only calculations utilizing a small bath ($N_k = 1$) converge to a ferromagnetic ground state. Despite a number of attempts, we have not succeeded in finding a suitable modification of the fitting function [Eq. (5)] that would reliably eliminate the nonmagnetic solution in the case of larger baths. Surely the nonmagnetic ground state would go away for large enough N_k without any change to Eq. (5), but that route is not feasible due to large computational demands. The problem is discussed further in the Appendix.

The impossibility of improving the description of the bath by doubling the number of bath orbitals has led us to reconsider the bath discretization strategy. We have replaced Eq. (5) with an alternative approach, namely, with the requirement of coincidence of the high-frequency asymptotics of $\hat{\mathcal{G}}_{\rm c}(z)$ and $\hat{\mathcal{G}}(z)$.[16,26] This method builds on the following algebra: The cluster Green's function $\hat{\mathcal{G}}_{\rm c}(z)$ can be written in an explicit form[27]

$$\mathcal{G}^{\rm c}_{m\sigma}(z) = \left(z - \epsilon_{m\sigma} - \sum_k \frac{V^2_{km\sigma}}{z - \epsilon_{km\sigma}} \right)^{-1} \tag{6}$$

whose expansion in powers of $1/z$ reads as

$$\mathcal{G}^{\rm c}_{m\sigma}(z) = \frac{1}{z} + \frac{\epsilon_{m\sigma}}{z^2} + \frac{\epsilon^2_{m\sigma} + \sum_k V^2_{km\sigma}}{z^3} + \frac{\epsilon^3_{m\sigma} + \sum_k V^2_{km\sigma}(\epsilon_{km\sigma} + 2\epsilon_{m\sigma})}{z^4} + \cdots . \tag{7}$$

The continuous Green's function $\hat{\mathcal{G}}(z)$ can be expressed in terms of the density of states $g(z)$, and the coefficients of the expansion in powers of $1/z$ are then given as moments of this density of states,

$$\mathcal{G}_{m\sigma}(z) = \int \frac{g_{m\sigma}(\epsilon)}{z-\epsilon}\, d\epsilon = \sum_{n=1}^{\infty} \frac{1}{z^n} \underbrace{\int \epsilon^{n-1} g_{m\sigma}(\epsilon)\, d\epsilon}_{M_{n-1}} . \tag{8}$$

In the case of $N_k = 2$ we have five parameters in $H^{(0)}_{\rm c}$ that carry the same indices m and σ, and thus we can match Eqs. (7) and (8) term by term up to $1/z^6$. For $N_k = 1$, the match is possible up to $1/z^4$ and the final expressions for the Hamiltonian parameters are quite simple and intuitive. They read as

$$\epsilon_{m\sigma} = M_1, \tag{9a}$$

$$V^2_{km\sigma} = \tilde{M}_2, \tag{9b}$$

$$\epsilon_{km\sigma} = \epsilon_{m\sigma} + \tilde{M}_3/\tilde{M}_2, \tag{9c}$$

where M_1 is the "center of mass" of $g_{m\sigma}$ and $\tilde{M}_n$ are the central moments of $g_{m\sigma}$,

$$\tilde{M}_n = \int (\epsilon - M_1)^n g_{m\sigma}(\epsilon)\, d\epsilon\,. \tag{10}$$

The hybridization amplitude $V_{km\sigma}$ is given by the second central moment $\tilde{M}_2$ that characterizes the width of $g_{m\sigma}$ which in turn measures the impurity-bath hopping.

The discretization method defined by Eqs. (7) and (8) is susceptible to the same nonmagnetic solution just as Eq. (5) was, but this time there is a straightforward remedy in the form of a modified definition of the moments M_n,

$$M_n = \frac{\int_{\epsilon_l}^{\epsilon_u} \epsilon^n g_{m\sigma}(\epsilon)\, d\epsilon}{\int_{\epsilon_l}^{\epsilon_u} g_{m\sigma}(\epsilon)\, d\epsilon}. \tag{11}$$

The lower cutoff ϵ_l is a purely technical matter; it is set to $\epsilon_l = -9$ eV, that is, below the $4s$ band. The upper cutoff ϵ_u avoids the unphysical solution by not allowing the bath orbitals to drift to too high energies.

The last component of the cluster Hamiltonian $\hat{H}_c$ that we have not discussed yet is the Coulomb interaction in the d shell. We use the spherically symmetric form

$$\hat{U} = \frac{1}{2} \sum_{\substack{mm'm''\\ m'''\sigma\sigma'}} U_{mm'm''m'''} \hat{d}^\dagger_{m\sigma} \hat{d}^\dagger_{m'\sigma'} \hat{d}_{m'''\sigma'} \hat{d}_{m''\sigma} - U_{\mathrm{H}} \sum_{m\sigma} \hat{d}^\dagger_{m\sigma} \hat{d}_{m\sigma}\,, \tag{12}$$

where the matrix $U_{mm'm''m'''}$ is parametrized by the Slater integrals $F_0 = 2$ eV, $F_2 = 8.2$ eV, and $F_4 = 5.2$ eV. These numerical values correspond to Coulomb $U = 2$ eV and exchange $J = 0.95$ eV. The term proportional to U_{H} represents a rigid shift of the impurity levels downward, $\epsilon_{m\sigma} \to \epsilon_{m\sigma} - U_{\mathrm{H}}$, and accounts for the fact that the d–d Coulomb interactions are already partially included in the LDA Hamiltonian $\hat{H}(\mathbf{k})$ in the form of a static mean field. Several formulas have been proposed to express the Hartree-like double-counting potential U_{H} in terms of the occupation numbers of the d orbitals,[28–30] but we treat U_{H} as a free parameter similarly to Ref. 31 since neither of the standard choices leads to satisfactory results.

The need for "undressing" the LDA quasiparticles is one of the reasons why we prefer to build the many-body description on the top of the spin-restricted LDA band structure. If we started from spin-polarized bands, the Hartree potential U_{H} would be polarized too, which would add complexity to the problem. The double counting would have to be spin dependent also in the LDA + DMFT implementations that take into account the feedback of the self-energy on $\hat{H}(\mathbf{k})$.[32,33]

Once the cluster Hamiltonian $\hat{H}_c$ is fully specified, the one-particle Green's function $\hat{G}_c \equiv \hat{G}_{\mathrm{imp}}[\hat{H}_c]$ can be calculated. We employ the band Lanczos method[34,35] that allows for a simultaneous evaluation of all relevant matrix elements at once. Off-diagonal elements are directly accessible too, although this functionality is not used in the application at hand. For the purpose of the Lanczos method, $\hat{G}_c$ is written as[36]

$$G^{\mathrm{c}}_{m\sigma}(z) = \frac{1}{Z}[G^{>}_{m\sigma}(z) + G^{<}_{m\sigma}(z)], \tag{13}$$

where the two parts are

$$G^{>}_{m\sigma}(z) = \sum_\psi e^{-\beta E_\psi} \langle\psi|\hat{d}_{m\sigma}(z + E_\psi - \hat{H}_c)^{-1}\hat{d}^\dagger_{m\sigma}|\psi\rangle,$$

$$G^{<}_{m\sigma}(z) = \sum_\psi e^{-\beta E_\psi} \langle\psi|\hat{d}^\dagger_{m\sigma}(z - E_\psi + \hat{H}_c)^{-1}\hat{d}_{m\sigma}|\psi\rangle.$$

The sums over the many-body eigenstates $|\psi\rangle$, $\hat{H}_c|\psi\rangle = E_\psi|\psi\rangle$, represent grand-canonical averages with the chemical potential equal zero, and $Z = \sum_\psi e^{-\beta E_\psi}$ stands for the corresponding partition function. The calculations are performed at low temperature $k_{\mathrm{B}}T = 1/\beta = 0.01$ eV so that only the ground state contributes to the sum over ψ most of the time. The eigenstate-eigenvalue pairs including all their degeneracies are found using the implicitly restarted Lanczos method as implemented in the ARPACK software package.[37]

III. RESULTS AND DISCUSSION

A. Ground-state properties

First we examine selected characteristics of the ground state and use them to estimate the double-counting potential U_{H}. Figure 1 shows the number of electrons in the d orbitals $n_d = n_{d\uparrow} + n_{d\downarrow}$ and the spin polarization of these orbitals $m_d = n_{d\uparrow} - n_{d\downarrow}$. The quantities calculated in the lattice and in the discretized impurity model are plotted side by side. They differ despite the DMFT iterations being converged in the sense that the cluster Hamiltonian H_c no longer changed in the successive steps. The differences would vanish if we solved the full continuous impurity model since Eq. (2b) would be exactly fulfilled in that case.

It turns out that n_d and m_d depend only weakly on the double-counting potential U_{H} when the latter is larger than approximately 14.5 eV. Below 14.5 eV the trend changes and the cluster quantities depart substantially from their lattice counterparts. Based on this observation we consider U_{H} below

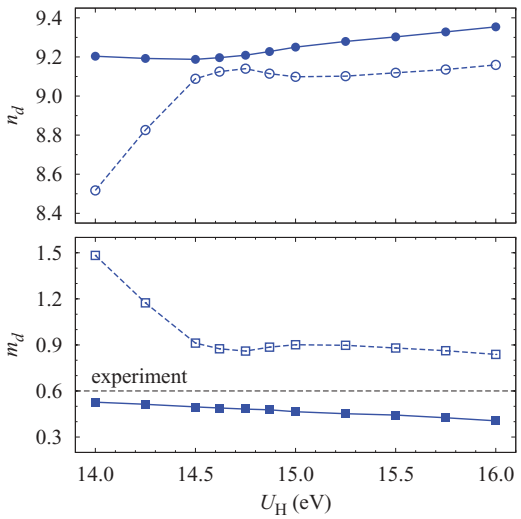

FIG. 1. (Color online) The occupation of the d orbitals n_d (top) and the spin polarization m_d (bottom) plotted as functions of the double-counting potential U_{H}. Empty symbols correspond to the cluster Green's function $\hat{G}_c$, full symbols to the lattice Green's function $\hat{G}$.

14.5 eV as inappropriate. We note in passing that the double counting in the so-called fully localized limit[29,30] $U_{\mathrm{H}}^{(\mathrm{FLL})} = U(n_d - 1/2) - J(n_d - 1)/2$ equals 13.2 eV for $n_d = 9$ and it is thus more than 1 eV too small to be applicable in our case. The so-called around mean-field form[28] of U_{H} provides an even smaller value.

The experimentally determined magnetization of the fcc nickel is approximately 0.6 μ_{B} per atom.[38] Our calculations slightly underestimate the magnetization even though the cluster solution, from which the spin-dependent self-energy is extracted, displays the maximal polarization characterized by $m_d = 5 - n_{d\downarrow}$.

The number of d electrons cannot be unambiguously defined in a solid and as such it does not represent a particularly useful measure of quality of our ground state. The d-band filling in nickel is often estimated as 9.4 per atom based on the measured magnetic moment and the assumption of the maximal d-shell polarization,[39] but reliability of this estimate is limited.

B. Valence-band spectrum

The d-orbital spectral function $\mathrm{Im}\sum_m [G_{m\sigma}(E - \mathrm{i}0)]/\pi$ represents a simple model for the angle-integrated photoemission intensity. We find that the spectra corresponding to the double-counting potential U_{H} in the range 15.0 ± 0.5 eV are only barely distinguishable, the result shown in Fig. 2 was obtained with $U_{\mathrm{H}} = 15$ eV. The calculated spectrum is relatively disappointing: the width of the main band (≈4.5 eV) as well as the exchange splitting are nearly identical to those obtained with the spin-polarized LDA and thus share the same poor agreement with experiments. The symmetry-resolved exchange splitting at the Fermi level is given directly by the self-energy and reads as

$$\Sigma_{e_g\uparrow}(E_{\mathrm{F}}) - \Sigma_{e_g\downarrow}(E_{\mathrm{F}}) \approx 0.3 \text{ eV}, \tag{14a}$$

$$\Sigma_{t_{2g}\uparrow}(E_{\mathrm{F}}) - \Sigma_{t_{2g}\downarrow}(E_{\mathrm{F}}) \approx 0.8 \text{ eV}. \tag{14b}$$

The d states near the Fermi level have predominantly the t_{2g} character, which results in the apparent exchange splitting of 0.6 eV that is visible as a shift between the top of the valence bands for the minority and majority spins (indicated with arrows in Fig. 2).

For a smaller bath, $N_k = 1$, we have also performed a series of calculations that utilized Eq. (5), instead of Eqs. (7) and (8), to discretize the impurity model. A representative result is shown in Fig. 3. The renormalization of the main band and the exchange splitting are more reasonable than they were in Fig. 2; the band width is approximately 3 eV and the exchange spitting is about 0.3 eV, both of which are close to the photoemission experiments.[1,2] Apparently the fitting at the Matsubara frequencies $i\omega_n$ is more sensitive to the behavior near the Fermi level than the method of moments [Eqs. (7) and (8)] and hence it results in a finer description of the low-energy spectral features. Notwithstanding, we *cannot* rely on the fitting at $i\omega_n$ because doubling the size of the bath to $N_k = 2$, which should improve the results, leads instead to an unphysical nonmagnetic solution as discussed in Sec. II.

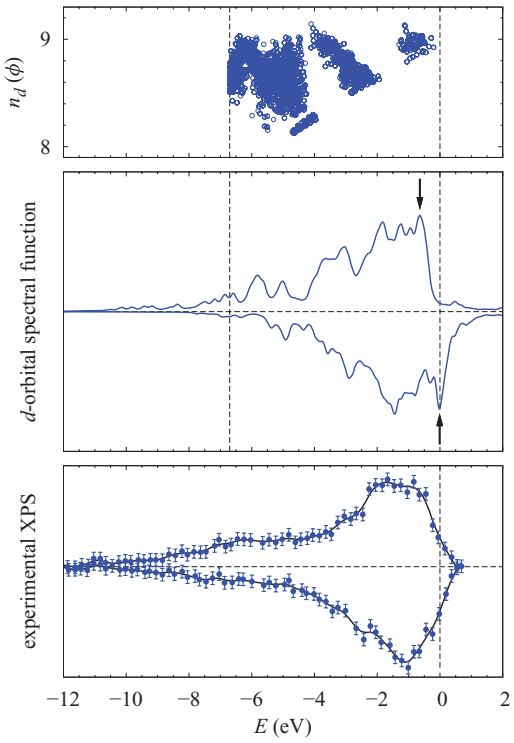

FIG. 2. (Color online) Spin-resolved d-orbital spectral function of bulk Ni obtained with $U_{\mathrm{H}} = 15$ eV (middle panel) in comparison with the valence-band x-ray photoemission spectrum (XPS) from Ref. 40 (bottom panel; the non-d background was approximately removed by shifting the spectra in the vertical direction so that they approach zero at high binding energies). The top panel shows the d-orbital occupation $n_d(\phi)$ in each of the first 5000 many-body final states $|\phi\rangle$ evaluated in the discretized impurity model.

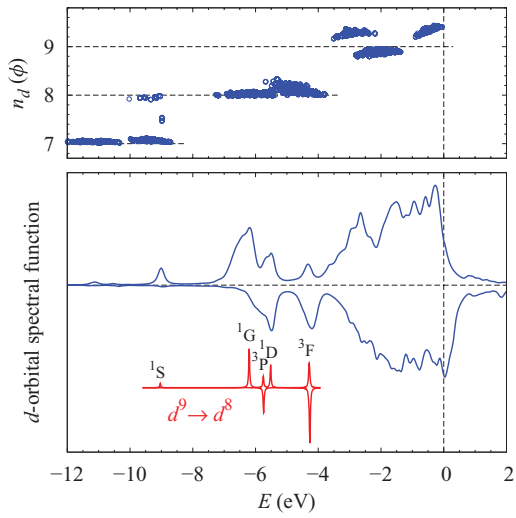

FIG. 3. (Color online) Spin-resolved d-orbital spectral function of bulk Ni that was obtained with the bath discretized using the least-squares fit at the Matsubara frequencies (bottom panel). The auxiliary impurity model contains only one bath orbital per each impurity orbital ($N_k = 1$). The atomic $d^9 \rightarrow d^8$ transitions are displayed at an arbitrary scale and position for comparison with the shape of the satellite. The upper panel shows the d-orbital occupation $n_d(\phi)$ in the final states $|\phi\rangle$ evaluated in the discretized impurity model.

C. Valence-band satellite

We identify the spectral features found below approximately −4.5 eV as the "6 eV satellite." It is strongly spin polarized in agreement with spin-resolved photoemission experiments.[40] For the results presented in Fig. 2, the energy-integrated satellite intensity is about three times larger for the majority spins than for the minority spins. Furthermore, the minority-spin states are located at reduced binding energies, which was also observed experimentally.[41] These two properties support the identification of the valence-band satellite with localized atomic-like transitions from the spin-polarized d^9 initial state (five majority spins and four minority spins) to the d^8 final states, that is, to states with two localized $3d$ holes.[9,42] An illustration of the atomic d^8 final-state multiplets is added to Fig. 3 for comparison. The singlet final states ^1D, ^1G, and ^1S exhibit a complete majority-spin polarization and lie deeper, the triplet states ^3F and ^3P carry a partial polarization in the opposite direction (66% of spin-down intensity and 33% of spin-up intensity[43]) and lie shallower.

In order to analyze the electronic states responsible for the satellite in more detail, we have evaluated the d-orbital occupation $n_d(\phi) = \sum_{m\sigma} \langle\phi|\hat{d}^\dagger_{m\sigma}\hat{d}_{m\sigma}|\phi\rangle$ in the final states $|\phi\rangle$ of the photoemission process that enter the Lehmann representation of the impurity Green's function as

$$G^<_{m\sigma}(z) = \sum_{\psi\phi} e^{-\beta E_\psi} \frac{\langle\psi|\hat{d}^\dagger_{m\sigma}|\phi\rangle\langle\phi|\hat{d}_{m\sigma}|\psi\rangle}{z - E_\psi + E_\phi}. \qquad (15)$$

Thus calculated $n_d(\phi)$ is aligned with the spectral functions in Figs. 2 and 3. In Fig. 3 (smaller bath) the satellite indeed corresponds to states with $n_d(\phi) \approx 8$, but the same is not quite true in the case of Fig. 2 (larger bath). Although $n_d(\phi)$ decreases as the binding energy increases in Fig. 2 as well, it is still considerably larger than eight in the satellite region where contributions from states with $n_d(\phi) \geqslant 8.5$ are not an exception. This enhancement of $n_d(\phi)$ is due to the impurity-bath hybridization: there are no bath levels with $\epsilon_{km\sigma}$ near the satellite in the smaller bath, whereas there are such bath levels in the larger bath. The extra hybridization causes a partial delocalization of at least one of the $3d$ holes, which is accompanied by the increased $n_d(\phi)$.

As mentioned in Sec. III B, our results are rather insensitive to a particular choice of the potential U_H as long as it exceeds a threshold of approximately 14.5 eV. For smaller U_H, the impurity orbitals in the cluster start to depopulate, which is accompanied by an increased intensity of the satellite. The same effect was observed in experiments on alloys of Ni with electropositive metals.[44,45]

IV. CONCLUSIONS

We have investigated the valence-band spectra of the ferromagnetic nickel within the LDA + DMFT framework. The auxiliary impurity model was discretized and then solved using the Lanczos method. The valence-band satellite and its spin dependence were reproduced in good agreement with spin-resolved photoemission experiments. The many-body renormalization of the $3d$ bands as well as the exchange splitting were found to be sensitive to the details of the bath discretization, which indicates that ten orbitals are probably not enough to approximate the bath of conduction electrons to a satisfactory accuracy. The diagonalization method as employed in this paper is adequate for recovering features of atomic origin located at high binding energies but it is apparently too crude to consistently capture the expected modification of the Fermi-liquid parameters at low binding energies.

ACKNOWLEDGMENTS

Financial support by the Deutsche Forschungsgemeinschaft through FOR 1346 is gratefully acknowledged. J. K. acknowledges financial support by the Alexander von Humboldt Foundation. A.P. acknowledges the Russian Foundation for Basic Research (Projects No. 10-02-00046, No. 10-02-91003, and No. 11-02-01443).

APPENDIX: MAGNETISM IN THE FINITE CLUSTER

Here we take a closer look at the issues that forced us to turn away from the standard bath-discretization strategy [Eq. (5)], and that necessitated the introduction of the cutoffs in Eq. (11). To illustrate the problem we use a simpler impurity model than we employed in Sec. III—we reduce the cluster to contain only one bath orbital per each impurity orbital, $N_k = 1$, and we assume spherical instead of cubic symmetry. Furthermore, we implement the Hamiltonian parameters used in Ref. 12, which gives us the opportunity to relate our calculations to this earlier study of electron correlations in nickel. The Slater integrals are $F_0 = 3.5$ eV, $F_2 = 9.79$ eV, and $F_4 = 6.08$ eV, and the impurity-bath hopping is $V_{km\sigma} = 0.7$ eV. The bath-level position $\epsilon_{km\sigma} \equiv \epsilon_\mathrm{b}$ is treated as a free parameter and the double-counting potential U_H is determined such that there are always nine electrons in the impurity d orbitals. The temperature is $k_\mathrm{B}T = 0.01$ eV as before.

The spin polarization is induced by a small magnetic field B coupled to the impurity spins. The coupling is described by an extra term in the cluster Hamiltonian,

$$\hat{H}^{(B)}_\mathrm{c} = \frac{B}{2}\sum_m (\hat{d}^\dagger_{m\uparrow}\hat{d}_{m\uparrow} - \hat{d}^\dagger_{m\downarrow}\hat{d}_{m\downarrow}).$$

The resulting polarization is plotted in Fig. 4 as a function of the bath position ϵ_b scanned across the Fermi level. The total number of electrons in the cluster is shown as well.

When the bath orbitals are sufficiently deep below the Fermi level, the bath is nearly full and a local magnetic moment is formed on the impurity. As the bath orbitals move up toward the Fermi level, the bath relatively quickly depopulates until it holds only a single electron. This electron, together with the other nine sitting in the impurity orbitals, forms a nonmagnetic d^{10} closed shell. This state then remains stable even when the bath is raised relatively high above the Fermi level. Only for $\epsilon_\mathrm{b} > 2.4V_{km\sigma} \approx 1.7$ eV the bath starts releasing the last electron and a magnetic ground state is restored. The larger cluster corresponding to $N_k = 2$ shows an analogous behavior, only the nonmagnetic solution occurs for 20 electrons in the cluster as there is an extra fully occupied shell of bath orbitals located deeper below the Fermi level.

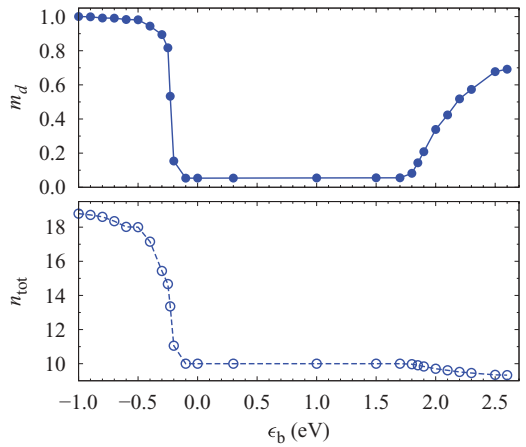

FIG. 4. (Color online) Spin polarization of the d shell m_d (top) and the total number of electrons in the whole cluster $n_{\rm tot}$ (bottom) as functions of the bath-level position $\epsilon_{\rm b}$.

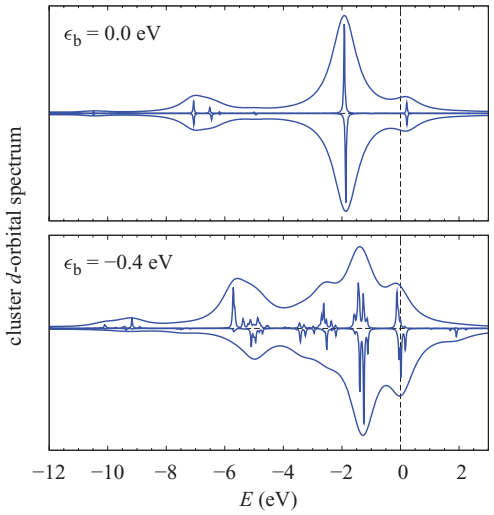

FIG. 5. (Color online) Spin-resolved d-orbital spectral function of a cluster with parameters taken from Ref. 12. A nonmagnetic state ($\epsilon_{\rm b} = 0$ eV, top panel) is compared to a magnetic solution ($\epsilon_{\rm b} = -0.4$ eV, bottom panel). The "envelopes" are calculated with a large Lorentz broadening of 0.5 eV.

It is clear that the nonmagnetic solution does not correctly describe the d shell and its environment in the ferromagnetic nickel. Elevating the bath orbitals high above the Fermi level in order to support a magnetic ground state does not look as a plausible remedy, which leaves us with the configuration where the bath states are nearly fully occupied and thereby model the nearly full d orbitals of the nickel atoms surrounding the "impurity" site. To prevent the cluster Hamiltonian to enter the nonrealistic regimes in the course of the DMFT iterations, we have introduced the upper cutoff ϵ_u in the integrals in Eq. (11). This cutoff does not allow the bath orbitals to drift too high and to lock into the nonmagnetic solution.

It is instructive to compare the spectral functions corresponding to the different cluster ground states. The top panel of Fig. 5 shows the spectrum obtained when the bath orbitals are placed right at the Fermi level $\epsilon_{\rm b} = 0$. The local moment induced by the external magnetic field is negligible in this case and the spectral function is nearly symmetric. The spectrum is practically identical to the result presented in Ref. 12 as it should be since we used the same parameters.

The spectrum corresponding to the bath orbitals lowered to -0.4 eV is plotted in the bottom panel of Fig. 5. The 6 eV satellite now has a shape similar to our DMFT solution as well as to the experimental data: the minority-spin component is less intense and is located at smaller binding energies.

*kolorenc@fzu.cz

[1] D. E. Eastman, F. J. Himpsel, and J. A. Knapp, Phys. Rev. Lett. **40**, 1514 (1978).
[2] W. Eberhardt and E. W. Plummer, Phys. Rev. B **21**, 3245 (1980).
[3] C. S. Fadley and D. A. Shirley, Phys. Rev. Lett. **21**, 980 (1968).
[4] Y. Baer, P. F. Hedén, J. Hedman, M. Klasson, C. Nordling, and K. Siegbahn, Solid State Commun. **8**, 517 (1970).
[5] S. Hüfner and G. K. Wertheim, Phys. Lett. A **47**, 349 (1974).
[6] S. Hüfner and G. K. Wertheim, Phys. Lett. A **51**, 299 (1975).
[7] P. C. Kemeny and N. J. Shevchik, Solid State Commun. **17**, 255 (1975).
[8] C. Guillot, Y. Ballu, J. Paigné, J. Lecante, K. P. Jain, P. Thiry, R. Pinchaux, Y. Pétroff, and L. M. Falicov, Phys. Rev. Lett. **39**, 1632 (1977).
[9] L. A. Feldkamp and L. C. Davis, Phys. Rev. Lett. **43**, 151 (1979).
[10] R. Clauberg, W. Gudat, E. Kisker, E. Kuhlmann, and G. M. Rothberg, Phys. Rev. Lett. **47**, 1314 (1981).
[11] R. H. Victora and L. M. Falicov, Phys. Rev. Lett. **55**, 1140 (1985).
[12] A. Tanaka, T. Jo, and G. A. Sawatzky, J. Phys. Soc. Jpn. **61**, 2636 (1992).
[13] D. R. Penn, Phys. Rev. Lett. **42**, 921 (1979).
[14] A. Liebsch, Phys. Rev. Lett. **43**, 1431 (1979).
[15] J. I. Igarashi, P. Unger, K. Hirai, and P. Fulde, Phys. Rev. B **49**, 16181 (1994).
[16] A. Georges, G. Kotliar, W. Krauth, and M. J. Rozenberg, Rev. Mod. Phys. **68**, 13 (1996).
[17] A. I. Lichtenstein, M. I. Katsnelson, and G. Kotliar, Phys. Rev. Lett. **87**, 067205 (2001).
[18] M. I. Katsnelson and A. I. Lichtenstein, Eur. Phys. J. B **30**, 9 (2002).
[19] J. Braun, J. Minár, H. Ebert, M. I. Katsnelson, and A. I. Lichtenstein, Phys. Rev. Lett. **97**, 227601 (2006).
[20] A. Grechnev, I. Di Marco, M. I. Katsnelson, A. I. Lichtenstein, J. Wills, and O. Eriksson, Phys. Rev. B **76**, 035107 (2007).
[21] D. Benea, J. Minár, L. Chioncel, S. Mankovsky, and H. Ebert, Phys. Rev. B **85**, 085109 (2012).
[22] O. K. Andersen, Phys. Rev. B **12**, 3060 (1975).
[23] M. Caffarel and W. Krauth, Phys. Rev. Lett. **72**, 1545 (1994).

[24] A. Privitera, M. Capone, and C. Castellani, Phys. Rev. B **81**, 014523 (2010).
[25] C. A. Perroni, H. Ishida, and A. Liebsch, Phys. Rev. B **75**, 045125 (2007).
[26] Q. Si, M. J. Rozenberg, G. Kotliar, and A. E. Ruckenstein, Phys. Rev. Lett. **72**, 2761 (1994).
[27] A. C. Hewson, *The Kondo Problem to Heavy Femions* (Cambridge University Press, Cambridge, 1993).
[28] V. I. Anisimov, J. Zaanen, and O. K. Andersen, Phys. Rev. B **44**, 943 (1991).
[29] M. T. Czyżyk and G. A. Sawatzky, Phys. Rev. B **49**, 14211 (1994).
[30] I. V. Solovyev, P. H. Dederichs, and V. I. Anisimov, Phys. Rev. B **50**, 16861 (1994).
[31] M. Karolak, G. Ulm, T. Wehling, V. Mazurenko, A. Poteryaev, and A. Lichtenstein, J. Electron Spectrosc. Relat. Phenom. **181**, 11 (2010).
[32] A. B. Shick, J. Kolorenč, A. I. Lichtenstein, and L. Havela, Phys. Rev. B **80**, 085106 (2009).
[33] K. Haule, C.-H. Yee, and K. Kim, Phys. Rev. B **81**, 195107 (2010).
[34] A. Ruhe, Math. Comput. **33**, 680 (1979).
[35] H.-D. Meyer and S. Pal, J. Chem. Phys. **91**, 6195 (1989).
[36] M. Capone, L. de' Medici, and A. Georges, Phys. Rev. B **76**, 245116 (2007).
[37] R. B. Lehoucq, D. C. Sorensen, and C. Yang, *ARPACK Users' Guide* (SIAM, Washington, DC, 1998).
[38] H. Danan, A. Herr, and A. J. P. Meyer, J. Appl. Phys. **39**, 669 (1968).
[39] N. F. Mott, Adv. Phys. **13**, 325 (1964).
[40] A. K. See and L. E. Klebanoff, Phys. Rev. B **51**, 11002 (1995).
[41] A. Kakizaki, K. Ono, K. Tanaka, K. Shimada, and T. Sendohda, Phys. Rev. B **55**, 6678 (1997).
[42] Y. Sakisaka, T. Komeda, M. Onchi, H. Kato, S. Masuda, and K. Yagi, Phys. Rev. Lett. **58**, 733 (1987).
[43] S. F. Alvarado and P. S. Bagus, Phys. Lett. A **67**, 397 (1978).
[44] J. Fuggle and Z. Zolnierek, Solid State Commun. **38**, 799 (1981).
[45] J. C. Fuggle, F. U. Hillebrecht, R. Zeller, Z. Zołnierek, P. A. Bennett, and C. Freiburg, Phys. Rev. B **27**, 2145 (1983).